

A fully-coupled discontinuous Galerkin method for two-phase flow in porous media with discontinuous capillary pressure

Peter Bastian

Heidelberg University, Interdisciplinary Center for Scientific Computing
Im Neuenheimer Feld 368, D-69120 Heidelberg, Germany
`peter.bastian@iwr.uni-heidelberg.de`

February 26, 2022

In this paper we formulate and test numerically a fully-coupled discontinuous Galerkin (DG) method for incompressible two-phase flow with discontinuous capillary pressure. The spatial discretization uses the symmetric interior penalty DG formulation with weighted averages and is based on a wetting-phase potential / capillary potential formulation of the two-phase flow system. After discretizing in time with diagonally implicit Runge-Kutta schemes the resulting systems of nonlinear algebraic equations are solved with Newton’s method and the arising systems of linear equations are solved efficiently and in parallel with an algebraic multigrid method. The new scheme is investigated for various test problems from the literature and is also compared to a cell-centered finite volume scheme in terms of accuracy and time to solution. We find that the method is accurate, robust and efficient. In particular no post-processing of the DG velocity field is necessary in contrast to results reported by several authors for decoupled schemes. Moreover, the solver scales well in parallel and three-dimensional problems with up to nearly 100 million degrees of freedom per time step have been computed on 1000 processors.

Keywords: Two-Phase Flow · Porous Medium · Discontinuous Galerkin · Algebraic Multigrid

1 INTRODUCTION

Modelling and simulation of multi-phase flow in porous media has important applications ranging from secondary oil recovery [62, 5] to nuclear waste repositories [19] and CO₂ sequestration [29]. In this paper we concentrate on the flow of two incompressible and immiscible phases as a basic model which reduces, upon certain manipulation of the equations,

to two coupled nonlinear, time-dependent partial differential equations of elliptic-parabolic type providing several formidable difficulties for the analysis as well as for the numerical solution.

One complication of the model that we do allow is heterogeneity in the capillary pressure function which can have a decisive effect on the flow of the fluids and requires careful numerical treatment [56, 57]. Modeling of two-phase flow with different capillary pressure curves in different parts of the domain (termed “discontinuous capillary pressure” in the following) has been studied extensively in the literature [16, 36, 33, 37]. The mathematically correct form of the interface conditions has been derived through a regularisation technique in [36]. Significant advances in the model analysis have been achieved in [17, 24, 25, 26].

The treatment of discontinuous capillary pressures in numerical simulators has been studied for around two decades in the context of a wide variety of different numerical schemes and is still an active field of research. Kueper and Frind [56, 57] used finite difference schemes and compared their numerical simulations against experimental results. Standard Galerkin and Petrov-Galerkin method are compared against upwind finite volume methods by Helmig and Huber in [50, 51]. The authors find that upwinding is crucial and that standard Galerkin and Petrov-Galerkin methods may produce unphysical results. Upwinding, however, implements the required interface conditions only approximately. Discontinuous capillary pressures in the context of various cell-centered finite volume schemes with two-point flux approximation are studied in [36, 27, 21] while an extension to multi-point flux on hexahedral, non-conforming meshes has been given recently in [72]. The vertex-centered fi-

nite volume method with an exact treatment of the interface conditions has been introduced in [6, 11] and has been extended to fractured porous media in [65]. The mixed finite element method is a very accurate, efficient and popular method for numerically solving heterogeneous elliptic problems. The extension of this method to two-phase flow with capillary pressure discontinuities has been presented for the multi-dimensional case in [52].

Discontinuous Galerkin (DG) finite element methods [30, 68, 34] are a class of non-conforming finite element schemes having several advantages: They are able to achieve higher order of convergence while being locally conservative, are able to handle full permeability tensors, unstructured, non-conforming meshes and can be used to increase the ratio of floating point operations to memory accesses which is becoming increasingly important for modern computer architectures. Moreover, DG schemes have been designed for elliptic [67, 3, 44], parabolic [31, 1, 12] and hyperbolic problems [32]. For a recent comparison of a wide range of discretization schemes for 3d elliptic benchmark problems see [46].

Application of DG methods to incompressible, two-phase flow started about 10 years ago with the work in [7, 14, 66, 55] which all use decoupled formulations where, per time step, first a pressure equation is solved and then the saturation is advanced by an explicit time-stepping scheme (also called IMPES: implicit pressure, explicit saturation). For the pressure equation primal DG methods based on symmetric (SIPG) or non-symmetric (NIPG) interior penalties (see [3]) are used. If the saturation equation is hyperbolic upwinding and limiters are used to remove unphysical oscillations and to ensure convergence to the correct solution. In [14] this is combined with an $H(\text{div})$ velocity reconstruction technique that has been introduced and analyzed in [13]. Eslinger [45] presented a decoupled scheme based on the local discontinuous Galerkin scheme (LDG, [31]) and a Kirchhoff transformation of the nonlinear diffusion terms which can handle compressible fluids as well as discontinuous capillary pressure. Decoupled formulations combining a mixed finite element method for the pressure equation with an explicit DG method for the saturation equation have been presented in [59, 52]. The paper of Hoteit and Firoozabadi [52] introduced a formulation of two-phase flow based on phase potentials and a new velocity variable that enables the treatment of discontinuous capillary pressures within a mixed method. The first fully coupled DG schemes for 2d horizontal two-phase flow have been put forward in [38, 68]. The authors compare two different formulations based on either total

fluid conservation or both phase conservation equations and do *not* use upwinding nor slope limiting. The implicit Euler method is used for time discretization. More recently, a decoupled DG scheme in one space dimension based on a global pressure / saturation formulation has been introduced in [40, 41]. Discontinuous capillary pressure functions and consequently discontinuities in global pressure as well as saturation are taken into account by a careful design of the penalty terms within an SIPG approach. Heterogeneity and anisotropy in absolute permeability is taken care of by weighted averages introduced in [44]. The authors emphasize that an $H(\text{div})$ reconstruction [42, 39] of total velocity is strictly required by the scheme and provide numerical evidence that unphysical oscillations occur if this is not done. The saturation equation is discretized in time by the *implicit* Euler method (albeit being decoupled) and upwinding but no limiters are employed. The first DG method for compositional two-phase flow has been presented by the same authors in [43].

Due to the incompressibility constraint any simulator for the two-phase flow system requires the solution of large, sparse linear systems. In the decoupled approach this is one system per time step while in the fully-coupled approach non-linear algebraic systems need to be solved iteratively resulting in the solution of several linear systems per time step. The multigrid method [49] is among the fastest iterative methods for solving linear systems of equations arising from the discretization of elliptic PDEs. Multigrid methods are most developed for the systems arising from low-order finite element and finite volume discretizations but in the last decade they have been extended to systems arising from DG discretizations. Geometric multigrid applied to DG for the Poisson equation is analyzed in [48, 22] while heterogeneous elliptic problems have been treated recently in [4] and smoothed aggregation multigrid solvers have been presented in [63, 61]

In this paper we present a fully-coupled symmetric interior penalty DG method for incompressible two-phase flow based on a formulation using wetting-phase potential and capillary potential as primary variables. As equations, total fluid conservation and conservation of the non-wetting phase with a reconstruction of the same velocity variable as in Hoteit and Firoozabadi [52] are used. Discontinuity in capillary pressure functions is taken into account by incorporating the interface conditions into the penalty terms for capillary potential. Heterogeneity in absolute permeability is treated by the weighted averages from [44, 40]. The higher-order DG discretization in space is complemented by higher-order diagonally im-

PLICIT Runge-Kutta methods in time. The large-scale linear systems arising within the Newton scheme per Runge-Kutta stage are solved with an algebraic multigrid method [15] based on subspace correction [73].

The rest of this paper is structured as follows: In section 2 we describe the two-phase flow model and the specific formulation used. The DG discretization and fully-coupled solution approach is introduced in section 3 while section 4 gives details about the algebraic multigrid solver for the linear systems. Section 5 reports numerical results on four test cases in several variants. A conclusion on the findings of this paper is provided in section 6.

2 TWO-PHASE FLOW MODEL

2.1 Model Formulation

The system of immiscible and incompressible flow of two phases $\alpha \in \{w, n\}$ in a domain $\Omega \subset \mathbb{R}^d$ and time interval $\Sigma = (0, T)$ reads:

$$\Phi \partial_t s_\alpha + \nabla \cdot v_\alpha = q_\alpha \quad \text{in } \Omega \times \Sigma, \quad (1a)$$

$$v_\alpha = -\lambda_\alpha K (\nabla p_\alpha - \rho_\alpha g \nabla d), \quad (1b)$$

$$p_n - p_w = \pi(s_w, x), \quad (1c)$$

$$s_w + s_n = 1. \quad (1d)$$

Here Φ is porosity, $s_\alpha(x, t)$, $p_\alpha(x, t)$ are the unknown saturation and pressure depending on position x and time t , v_α is the velocity of phase α , q_α are external sources and sinks, phase mobility $\lambda_\alpha = k_{r\alpha}(s_\alpha)/\mu_\alpha$ is relative permeability divided by dynamic viscosity, $K(x)$ is the absolute permeability tensor, ρ_α is (constant) mass density, g is the gravitational acceleration, $d(x)$ is depth and $\pi(s_w, x)$ is the capillary pressure - saturation relationship. We are particularly interested in the case of discontinuous capillary pressure where the dependence of $\pi(s_w, x)$ on the position x is discontinuous. This results in discontinuous saturation requiring special treatment [36, 33, 11].

A large variety of formulations of the two-phase flow system (1) have been proposed in the literature based on the following options:

1. Provided the algebraic system (1c), (1d) is invertible, two out of the four unknown functions p_w, p_n, s_w and s_n can be eliminated. This results in various pressure-saturation and pressure-pressure formulations.
2. The system of variables can be transformed into new variables resulting in global pressure based formulations [28, 40] and potential based formulations [52].

3. The PDE system (1a), (1b) can be taken as is or rearranged into a total fluid conservation equation coupled to one phase conservation equation. Either the phase velocity or the total velocity $v_t = v_w + v_n$ can be used in the remaining phase conservation equation.

Our formulation of the system (1) is based in part on the formulation given by Hoteit and Firoozabadi in [52]. Introducing the wetting-phase potential and capillary potential as primary variables

$$\phi_w = p_w - \rho_w g d, \quad \phi_c = p_n - p_w - (\rho_n - \rho_w) g d \quad (2)$$

we can write the total velocity and the non-wetting phase velocity as

$$v_t = v_a - \lambda_n K \nabla \phi_c, \quad (3)$$

$$v_n = f_n v_a - \lambda_n K \nabla \phi_c, \quad (4)$$

with the newly introduced velocity

$$v_a = -\lambda_t K \nabla \phi_w, \quad (5)$$

the total mobility $\lambda_t = \lambda_w + \lambda_n$ and the fractional flow function $f_n = \lambda_n / \lambda_t$. Note that saturation can be computed from the capillary potential provided the capillary pressure-saturation relationship is invertible at a given position x :

$$s_w(x, t) = \psi(\phi_c(x, t) + (\rho_n - \rho_w) g d(x), x) \quad (6)$$

where $\psi(\pi(s_w, x), x) = s_w$. Summing (1a) for $\alpha = w, n$ and using (1d) we obtain the total fluid conservation equation

$$\nabla \cdot v_t = q_t \quad (7)$$

where $q_t = q_w + q_n$. As second equation we use conservation of the nonwetting-phase:

$$\Phi \partial_t (1 - \psi(\phi_c)) + \nabla \cdot v_n = q_n. \quad (8)$$

Inserting (3) into (7) and (4) into (8) we obtain the final form of our formulation:

$$-\nabla \cdot (\lambda_t K \nabla \phi_w + \lambda_n K \nabla \phi_c) = q_t, \quad (A)$$

$$-\Phi \partial_t \psi(\phi_c) + \nabla \cdot (f_n v_a - \lambda_n K \nabla \phi_c) = q_n. \quad (B)$$

The first equation is elliptic with respect to ϕ_w with non-degenerate coefficient λ_t depending on ϕ_c . The second equation is non-linear degenerate parabolic in ϕ_c and is coupled to the first equation through the velocity v_a . In regions where $f_n = 1$ (i.e. $s_n = 1$) the two equations (A), (B) coincide and the system becomes singular. Therefore we require that the wetting phase does not vanish.

Note that the differences of this formulation to the one given in [52] are two-fold: (i) we use capillary potential instead of saturation as a primary variable and (ii) we use conservation of non-wetting phase instead of conservation of wetting phase

$$\Phi \partial_t s_w + \nabla \cdot (f_w v_a) = q_w \quad (9)$$

which is always hyperbolic. In case of dominating capillary diffusion these diffusive effects need to be incorporated via the velocity field v_a whereas in our formulation a diffusion term is present. Therefore we consider our formulation more suited to the case of dominating capillary diffusion. On the other hand, if capillary diffusion effects are small, we need to rely on the non-wetting phase flow being in the same direction as the wetting-phase. An advantage of pressure-pressure formulations is that part of the nonlinearity is moved from the diffusion term to the time derivative and that they provide a set of persistent variables for two-phase compositional flow in case of phase appearance and disappearance [60].

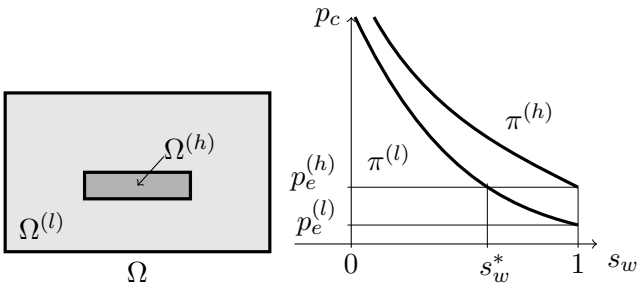
The equations (A), (B) are supplemented by boundary conditions

$$\begin{aligned} \phi_w &= \Phi_w & \text{on } \Gamma_w^D, & & v_t \cdot \nu &= J_t & \text{on } \Gamma_w^N, \\ \phi_c &= \Phi_c & \text{on } \Gamma_n^D, & & v_n \cdot \nu &= J_n & \text{on } \Gamma_n^N \end{aligned}$$

with Γ_w^D having non-zero measure and initial condition $\phi_c(x, 0) = \phi_c^0(x)$.

2.2 Interface Conditions

We assume the domain Ω is partitioned into subdomains $\Omega^{(i)}$ with different capillary pressure saturation relationships: $\pi(s_w, x) = \pi^{(i)}(s_w) \forall x \in \Omega^{(i)}$. For illustration consider two subdomains $\Omega^{(l)}$, $\Omega^{(h)}$ with corresponding curves $\pi^{(l)}$, $\pi^{(h)}$ of Brooks-Corey [23] type and $p_e^{(l)} = \pi^{(l)}(1) < p_e^{(h)} = \pi^{(h)}(1)$, i.e. $\pi^{(l)}$ having a smaller entry pressure:



In [36] it was derived through a regularization argument that at the interface of the two regions capillary pressure $p_c = p_n - p_w$ is continuous if, evaluated from the region $\Omega^{(l)}$, it is larger than the entry pressure of the region $\Omega^{(h)}$. This corresponds to a critical saturation s_w^* given by $\pi^{(l)}(s_w^*) = p_e^{(h)}$. Otherwise capillary

pressure is discontinuous and evaluated from the region $\Omega^{(h)}$ is equal to the entry pressure. Saturation is always discontinuous and takes on the two values $s_w^{(l)}$, $s_w^{(h)}$ given by:

$$\begin{cases} \pi^{(h)}(s_w^{(h)}) = \pi^{(l)}(s_w^{(l)}) & \text{if } \pi^{(l)}(s_w^{(l)}) \leq p_e^{(h)} \\ \pi^{(h)}(s_w^{(h)}) = p_e^{(h)} & \text{else} \end{cases} \quad (10)$$

In addition, wetting-phase pressure is continuous (assuming the wetting phase is always present) and the fluxes in normal direction of both phases (and consequently the total flux) are continuous at the interface.

The interface condition (10) can be reformulated in terms of the capillary potential ϕ_c by defining the entry potentials $\phi_c^{(i)}(x) = p_e^{(i)} - (\rho_n - \rho_w)gd(x)$ and setting:

$$\begin{cases} \phi_c^{(h)} = \phi_c^{(l)} & \text{if } \phi_c^{(l)} \geq \phi_e^{(h)} \\ \phi_c^{(h)} = \phi_e^{(h)} & \text{if } \phi_c^{(l)} < \phi_e^{(h)} \end{cases} \quad (11)$$

3 DISCONTINUOUS GALERKIN DISCRETIZATION

3.1 Notation

For the formulation of the DG discretization we employ the notation of [40]. By $\{\mathcal{T}_h\}_{h>0}$ we denote a family of shape regular triangulations of the domain Ω consisting of elements T which are either simplices or parallelipeds (this condition is only introduced for ease of notation) in $d = 1, 2, 3$ space dimensions. The diameter of T is h_T and ν_T is its unit outer normal vector. F is an interior face if it is the intersection of two elements $T^-(F), T^+(F) \in \mathcal{T}_h$ and F has non-zero measure in \mathbb{R}^d . All interior faces are collected in the set \mathcal{F}_h^i . Likewise, F is a boundary face if it is the intersection of some $T^-(F) \in \mathcal{T}_h$ with $\partial\Omega$ and has non-zero measure. All boundary faces make up the set $\mathcal{F}_h^{\partial\Omega}$ and we set $\mathcal{F}_h = \mathcal{F}_h^i \cup \mathcal{F}_h^{\partial\Omega}$. The diameter of $F \in \mathcal{F}_h$ is h_F and with each $F \in \mathcal{F}_h$ we associate a unit normal vector ν_F oriented from $T^-(F)$ to $T^+(F)$ in case of interior faces and coinciding with $\nu_{T^-(F)}$ in case of boundary faces.

It is assumed that the finite element mesh \mathcal{T}_h resolves the boundaries of the subdomains $\Omega^{(i)}$. By $\mathcal{F}_h^\Gamma \subseteq \mathcal{F}_h^i$ we denote the interior faces located at media discontinuities. For any face $F \in \mathcal{F}_h^\Gamma$ the normal direction ν_F is chosen such that it is oriented from the element with higher entry pressure to the element with lower entry pressure.

The DG finite element space of degree p on the mesh \mathcal{T}_h is

$$V_h^p = \{v \in L^2(\Omega) : \forall T \in \mathcal{T}_h, v|_T \in \mathcal{P}_p\} \quad (12)$$

where \mathcal{P}_p is either \mathbb{P}_p , the set of polynomials of total degree p or \mathbb{Q}_p , the set of polynomials of maximum

degree p . A function $v \in V_h^p$ is two-valued on an interior face $F \in \mathcal{F}_h^i$ and by v^- we denote the restriction from $T^-(F)$ and by v^+ the restriction from $T^+(F)$. For any point $x \in F \in \mathcal{F}_h^i$ we define the jump

$$[[v]](x) = v^-(x) - v^+(x) \quad (13)$$

and the weighted average

$$\{v\}_\omega(x) = \omega^- v^-(x) - \omega^+ v^+(x) \quad (14)$$

for some weights $\omega^- + \omega^+ = 1$, $\omega^\pm \geq 0$. A particular choice of the weights depending on the absolute permeability tensor K has been introduced in [35, 44]. Assuming that K^\pm is constant on $T^\pm(F)$ they set

$$\omega^- = \frac{\delta_{K\nu}^+}{\delta_{K\nu}^- + \delta_{K\nu}^+}, \quad \omega^+ = \frac{\delta_{K\nu}^-}{\delta_{K\nu}^- + \delta_{K\nu}^+}$$

with $\delta_{K\nu}^\pm = \nu_F^t K^\pm \nu_F$. The definitions of jump and average are extended to $x \in F \in \mathcal{F}_h^{\partial\Omega}$:

$$[[v]](x) = \{v\}_\omega(x) = v^-(x). \quad (15)$$

Finally, we denote for any domain Q by

$$(v, w)_Q = \int_Q v \cdot w \, dx$$

the L^2 scalar product of two (possibly vector-valued) functions, by $|Q| = (1, 1)_Q$ the measure of the set Q and by $\langle a, b \rangle = 2ab/(a+b)$ the harmonic mean of two numbers.

3.2 Total Fluid Conservation Equation

The discrete weak form defining the DG method for the total fluid conservation equation (A) is given for a test function w and fixed time t by

$$\begin{aligned} a_h(\phi_{wh}, \phi_{ch}, w) = & \sum_{T \in \mathcal{T}_h} (\lambda_t K \nabla \phi_{wh} + \lambda_n K \nabla \phi_{ch}, \nabla w)_T \\ & - \sum_{F \in \mathcal{F}_h^i \cup \mathcal{F}_h^{Dw}} (\nu_F \cdot \{\lambda_t K \nabla \phi_{wh} + \lambda_n K \nabla \phi_{ch}\}_\omega, [[w]])_F \\ & - \theta \sum_{F \in \mathcal{F}_h^i \cup \mathcal{F}_h^{Dw}} (\nu_F \cdot \{\lambda_t K \nabla w\}_\omega, [[\phi_{wh}]])_F \\ & + \sum_{F \in \mathcal{F}_h^i \cup \mathcal{F}_h^{Dw}} \gamma_{F,w} ([[w]], [[\phi_{wh}]])_F \end{aligned} \quad (16)$$

where we have split the domain boundary into Dirichlet and Neumann parts

$$\begin{aligned} \mathcal{F}_h^{D\alpha} &= \{F \in \mathcal{F}_h^{\partial\Omega} : F \subseteq \Gamma_\alpha^D\}, \\ \mathcal{F}_h^{N\alpha} &= \{F \in \mathcal{F}_h^{\partial\Omega} : F \subseteq \Gamma_\alpha^N\} \end{aligned}$$

and $\theta \in \{-1, 0, +1\}$ results in the non-symmetric, incomplete and symmetric version of the interior penalty DG method. The penalty factor $\gamma_{F,w}$ is crucial for the performance of the method and is chosen for interior faces as

$$\gamma_{F,w} = m \langle \lambda_t^- \delta_{K\nu}^-, \lambda_t^+ \delta_{K\nu}^+ \rangle \frac{p(p+d-1)|F|}{\min(|T^-(F)|, |T^+(F)|)}$$

and for boundary faces as

$$\gamma_{F,w} = m \lambda_t^- \delta_{K\nu}^- \frac{p(p+d-1)|F|}{|T^-(F)|}$$

with a user-defined parameter m . A typical choice is $m = 20$ for the examples shown below. The definition of the penalty parameter takes into account the coefficient of the elliptic equation, space dimension, polynomial degree and element form. It combines the choices from [35, 44] and [53].

The right hand side linear form incorporating source/sink term, Dirichlet and Neumann boundary conditions is

$$\begin{aligned} l_h(w) = & \sum_{T \in \mathcal{T}_h} (q, w)_T - \sum_{F \in \mathcal{F}_h^{Nw}} (J_t, w)_F \\ & - \theta \sum_{F \in \mathcal{F}_h^{Dw}} (\nu_F \cdot (\lambda_t K \nabla w), \Phi_w)_F \\ & + \sum_{F \in \mathcal{F}_h^{Dw}} \gamma_{F,w} (w, \Phi_w)_F \end{aligned} \quad (17)$$

The transport equation equation (A) is coupled to the equation for total fluid conservation through the velocity v_a defined in (5). Within an element T the discrete approximation of v_a is computed from the discrete function ϕ_{wh} . At interior and boundary faces F its normal component is computed as follows:

$$V_a = \begin{cases} \gamma_{F,w} [[\phi_{wh}]] - \nu_F \cdot \{\lambda_t K \nabla \phi_{wh}\}_\omega & F \in \mathcal{F}_h^i \\ \gamma_{F,w} (\phi_{wh} - \Phi_w) - \nu_F \cdot \lambda_t K \nabla \phi_{wh} & F \in \mathcal{F}_h^{Dw} \\ -\nu_F \cdot \lambda_t K \nabla \phi_{wh} & F \in \mathcal{F}_h^{Nw} \end{cases}.$$

We emphasize that the velocity field used in this way in the transport equation is not in $H(\text{div}, \Omega)$.

3.3 Non-wetting phase conservation equation

In order to solve the time-dependent problem we follow the “method of lines” approach discretizing first in space and then in time. The discrete weak formulation for the spatial derivatives of the right hand side

of equation (B) then reads:

$$\begin{aligned}
b_h(\phi_{wh}, \phi_{ch}, z) = & \\
& - \sum_{T \in \mathcal{T}_h} (f_n v_a - \lambda_n K \nabla \phi_{ch}, \nabla z)_T \\
& + \sum_{F \in \mathcal{F}_h^i \cup \mathcal{F}_h^{Dn}} (\langle f_n^{\uparrow, -}, f_n^{\uparrow, +} \rangle V_a, \llbracket z \rrbracket)_F \\
& - \sum_{F \in \mathcal{F}_h^i \cup \mathcal{F}_h^{Dn}} (\nu_F \cdot \{\lambda_n K \nabla \phi_{ch}\}_\omega, \llbracket z \rrbracket)_F \quad (18) \\
& - \theta \sum_{F \in \mathcal{F}_h^i \cup \mathcal{F}_h^{Dn}} (\nu_F \cdot \{\lambda_n K \nabla z\}_\omega, J(\phi_{ch}))_F \\
& + \sum_{F \in \mathcal{F}_h^i \cup \mathcal{F}_h^{Dn}} \gamma_{F,n}(\llbracket z \rrbracket, J(\phi_{ch}))_F
\end{aligned}$$

In line 3, $f_n^{\uparrow, \pm}$ denotes the upwind evaluation of the fractional flow function which is obtained as follows. First, capillary potential is evaluated through upwinding

$$\phi_{ch}^{\uparrow} = \begin{cases} \phi_{ch}^- & V_a \geq 0 \\ \phi_{ch}^+ & \text{else} \end{cases}. \quad (19)$$

Then the saturations on either side are evaluated by inverting the corresponding capillary pressure-saturation function

$$s_w^{\uparrow, \pm}(x, t) = \psi^{\pm}(\phi_{ch}^{\uparrow} + (\rho_n - \rho_w)gd(x), x) \quad (20)$$

and with these the fractional flow function is computed on either side

$$f_n^{\uparrow, \pm} = \frac{\frac{k_{rn}^{\pm}(1-s_w^{\uparrow, \pm})}{\mu_n}}{\frac{k_{rw}^{\pm}(s_w^{\uparrow, \pm})}{\mu_w} + \frac{k_{rn}^{\pm}(1-s_w^{\uparrow, \pm})}{\mu_n}}. \quad (21)$$

Then in line 3 of equation (18) the flux is computed by taking the harmonic average of the two values of the fractional flow function on either side of the face.

In order to incorporate the interface condition (11) for capillary potential the penalty terms make use of the extended jump function

$$J(\phi_{ch}) = \begin{cases} \phi_{ch}^{(h)} - \phi_{ch}^{(l)} & \phi_{ch}^{(l)} \geq \phi_e^{(h)}, F \in \mathcal{F}_h^\Gamma \\ \phi_{ch}^{(h)} - \phi_e^{(h)} & \phi_{ch}^{(l)} < \phi_e^{(h)}, F \in \mathcal{F}_h^\Gamma \\ \phi_{ch}^- - \phi_{ch}^+ & F \in \mathcal{F}_h^i \setminus \mathcal{F}_h^\Gamma \\ \phi_{ch}^- & F \in \mathcal{F}_h^{Dn} \end{cases}.$$

It enforces (11) (weakly) at media discontinuities and defaults to the standard jump term at all other faces.

The factor used in the interior penalty term now employs the arithmetic average of mobilities

$$\gamma_{F,n} = m \frac{\lambda_n^- + \lambda_n^+}{2} \langle \delta_{K\nu}^-, \delta_{K\nu}^+ \rangle \frac{p(p+d-1)|F|}{\min(|T^-(F)|, |T^+(F)|)}$$

which is important to get the correct front propagation in case of discontinuous initial conditions, cf. the discussion in [41]. The user-defined parameter m is typically chosen to be the same as for the total fluid conservation equation.

Finally, the right hand side linear form for the transport equation reads:

$$\begin{aligned}
r_h(z) = & \sum_{T \in \mathcal{T}_h} (q_n, z)_T - \sum_{F \in \mathcal{F}_h^{Nn}} (J_n, z)_F \\
& - \theta \sum_{F \in \mathcal{F}_h^{Dn}} (\nu_F \cdot (\lambda_n K \nabla z), \Phi_c)_F \quad (22) \\
& + \sum_{F \in \mathcal{F}_h^{Dn}} \gamma_{F,w}(z, \Phi_c)_F
\end{aligned}$$

3.4 Fully-coupled Solution approach

Following the method of lines approach the semi-discrete weak formulation now consists of the following problem: Find $\phi_{wh}(t), \phi_{ch}(t) : \Sigma \rightarrow V_h^p$ such that

$$\begin{aligned}
a_h(\phi_{wh}(t), \phi_{ch}(t), w) + \partial_t (\Phi(1 - \psi(\phi_{ch})), z)_\Omega \\
+ b_h(\phi_{wh}, \phi_{ch}, z) = l_h(w) + r_h(z) \quad (23)
\end{aligned}$$

for all $t \in \Sigma$ and $w, z \in V_h^p$. This equation comprises a large system of ordinary differential equations that is now discretized using diagonally implicit Runge-Kutta schemes. In particular, we employ the one step θ scheme which includes the implicit Euler and the Crank-Nicolson method and the Alexander schemes of order two and three described in [2].

Within each Runge-Kutta stage a large, nonlinear system of algebraic equations needs to be solved. This is done iteratively using Newton's method with line search globalization strategy and inexact (iterative) solution of the Jacobian system, see [11] for details. The Jacobians are generated numerically using first-order finite differences. In the following section we describe how the linear systems are solved.

4 SOLUTION OF LINEAR SYSTEMS

Let the linear system that is to be solved in each step of Newton's method be denoted by

$$Ax = b. \quad (24)$$

The matrix A is large, sparse and contains a block that stems from the discretization of an elliptic PDE with varying coefficients [11]. Therefore, the condition number is expected to be of order $\kappa(A) = O(h^{-2})$ which requires robust and efficient preconditioners to

be able to solve large-scale problems (see Section 5.4.4 for a quantitative assessment of this claim).

Multigrid methods are among the most efficient preconditioners for solving linear systems arising from the discretization of elliptic and parabolic PDEs [70]. In particular, algebraic multigrid is well suited to handle problems with varying coefficients [69]. Our preconditioner is based on the aggregation-based algebraic multigrid variant introduced independently by several authors in the 1990s [20, 71, 64]. Features of this method are its robustness for elliptic problems with varying coefficients, its applicability to systems of partial differential equations and its parallel scalability to a large number of processors [18]. A comparison of geometric multigrid and two algebraic multigrid variants (including our implementation) for large-scale anisotropic elliptic problems has been given recently in [58].

Although algebraic multigrid methods may be constructed that can directly be applied to linear systems arising from discontinuous Galerkin discretizations [54] our method exploits the fact that the standard conforming finite element space

$$W_h = \{v \in C^0(\Omega) : \forall T \in \mathcal{T}_h, v|_T \in \mathcal{P}_1\} \quad (25)$$

is a subspace of the DG finite element space V_h^p (provided the mesh is conforming). Since low-frequency errors can be represented well in W_h it is sufficient to apply a standard single-grid preconditioner to the fine grid DG system and combine it multiplicatively with an algebraic multigrid preconditioner seeking a correction in the subspace W_h in the sense of [73]. This method has been discussed in [15] for heterogeneous elliptic problems in a sequential implementation. Here it is applied to the full two-phase flow problem in a parallel implementation.

The error propagation matrix E of a generic linear iterative method $x^{(k+1)} = x^{(k)} + B(b - Ax^{(k)})$ for solving (24) employing the preconditioner B is given by $E = I - BA$. The error propagation matrix E_C of the combined AMG/DG preconditioner can be written as

$$E_C = (I - B_{DG}A)^{\nu_2} (I - R^T B_{AMG} R A) (I - B_{DG})^{\nu_1} \quad (26)$$

where B_{DG} is a single grid preconditioner for the DG system A , e.g. block Gauß-Seidel, block SSOR or block ILU with one block corresponding to all degrees of freedom associated with a mesh element. The entries of the restriction matrix R are given by the representation of the basis functions φ_i of W_h w.r.t. the basis functions ψ_j of V_h^p :

$$\varphi_i^{CG} = \sum_{j=1}^{n_{DG}} r_{ij} \psi_j^{DG}. \quad (27)$$

Finally, B_{AMG} is the AMG preconditioner for the matrix

$$A_{CG} = R A R^T.$$

The combined preconditioner can be derived in a fully algebraic way except the step (27) where information about the finite element basis functions is needed.

5 NUMERICAL RESULTS

5.1 Remarks on the Implementation

All methods discussed in this paper have been realized within the *Distributed and Unified Numerics Environment (DUNE)* [9, 8] and DUNE-PDELab [10]. DUNE is a flexible software framework that provides standardized interfaces to various parallel, hierarchical mesh representations, sparse linear algebra operations and finite element basis functions. The DUNE-PDELab module, which is based on the DUNE framework, allows the implementation of discretization schemes with relatively small coding effort (e.g. the complete DG scheme for two-phase flow takes less than 1000 lines of C++ code) and provides time discretizations and solvers in a reusable form.

5.2 Test Case 1: Van Duijn-De Neef Problem

In [37] the authors derived an analytical solution for a one-dimensional two-phase flow problem with heterogeneous capillary pressure. This problem has been used as a test problem in [52, 40]. Here we use the same parameters as Ern et al. in [40].

The domain $\Omega = (0, 1.2)$ is divided into two subdomains $\Omega^{(l)} = (0, 0.6)$ and $\Omega^{(r)} = (0.6, 1.2)$. The parameters for the two-phase problem are $\Phi = 1$, $\rho_w, \rho_n = 1$, $\mu_w, \mu_n = 1$. Relative permeabilities are of Brooks-Corey type [23] with $\lambda = 2$ and are identical in both subdomains:

$$k_{rw}(s_w) = s_w^{\frac{2+3\lambda}{\lambda}}, \quad k_{rn}(s_n) = s_n^2 \left(1 - (1 - s_n)^{\frac{2+\lambda}{\lambda}}\right).$$

In the implementation we set $k_{r\alpha} = 0$ if $s_\alpha < 0$ and $k_{r\alpha} = 1$ if $s_\alpha > 1$. Absolute permeability is heterogeneous. For test case 1a we set

$$K^{(l)} = 1, \quad K^{(r)} = 0.25$$

while for test case 1b we set

$$K^{(l)} = 1, \quad K^{(r)} = 0.64.$$

The capillary pressure function is also of Brooks-Corey type with $\lambda = 2$ in both subdomains

$$\pi(s_w, x) = p_e(x) s_w^{-1/\lambda} \quad (28)$$

and entry pressures given by $p_e(x) = \sqrt{1/K(x)}$.

Our formulation is based on the inverse of π which is regularized by replacing it with straight lines if $p_c < p_e$ or $p_c > Rp_e$ for some parameter $R > 1$:

$$\psi(p_c) = \begin{cases} 1 - \frac{\lambda}{p_e}(p_c - p_e) & p_c < p_e \\ \frac{1}{R^\lambda} - \frac{\lambda(p_c - Rp_e)}{R^{1+\lambda}p_e} & p_c > Rp_e \\ (p_e/p_c)^\lambda & \text{else} \end{cases} \quad (29)$$

We used $R = 4$ for test case 1a and $R = 6$ for test case 1b.

As boundary conditions we set $\phi_{wh}(0) = 0$, $\phi_{ch}(0) = 1 + 10^{-4}$ and $\nu \cdot v_t(1.2) = 0$, $\nu \cdot v_n(1.2) = 0$. The initial condition was $\phi_{wh}(x) = 0$, $\phi_{ch}(x) = 1 + 10^{-4}$ for $x \in \Omega^{(l)}$ and $\phi_{ch}(x) = 1.5R$ for $x \in \Omega^{(r)}$ (which corresponds to $s_w = 0$).

Numerical results for test case 1a/b are shown in Figure 1 at time $t = 1$ for three different spatial meshes employing 128, 256 and 512 equidistant elements. In all computations polynomial degree $p = 1$ for both variables and the second order Alexander scheme in time has been used. The figure shows excellent agreement of the numerical solution with the analytical solution even on the coarsest mesh. Comparing with the results given in [40] we find that our solution is already more accurate on the coarse meshes. Note that in [40] only the saturation equation is solved based on a fractional flow formulation and equidistant time steps were taken. In our simulations we solve the fully-coupled two phase problem where the time step size was chosen adaptively by the algorithm depending on the convergence of the Newton method. The actual number of time steps taken is reported in Table 1. The average time step size corresponds roughly to the size of the time steps taken in [40].

Figure 1 shows that the media discontinuity is captured well by the scheme without any oscillations. The second row of Figure 1 shows details of the solutions in the vicinity of the free boundary. The results indicate that the scheme converges towards the analytic solution and the steep front is well captured. There are small oscillations at the free boundary that are reduced as the mesh is refined.

5.3 Test Case 2: Ern et al. Problem

This problem is again taken from [40] where it was used to illustrate the importance of the $H(\text{div})$ reconstruction of total velocity in the decoupled scheme based on a fractional flow formulation. Here we use it to illustrate that such a reconstruction is *not* necessary in our fully-coupled approach. Note, that in [41] a corrigendum concerning this test case was published.

Table 1: Number of time steps for test case 1 to compute the time interval $(0, 1)$.

N	Δt_{\max}	$k_r = 0.64$	$k_r = 0.25$
128	$1 \cdot 10^{-2}$	187	184
256	$5 \cdot 10^{-3}$	296	282
512	$2.5 \cdot 10^{-3}$	484	497

The domain $\Omega = (0, 2)$ is one-dimensional and is partitioned into two subdomains $\Omega^{(l)} = (0, 1)$ and $\Omega^{(r)} = (1, 2)$. The parameters are $\Phi = 0.2$, $\rho_w, \rho_n = 1$, $\mu_w, \mu_n = 1$ and $K = 1$. Relative permeabilities are of Brooks-Corey type with $\lambda = 2$ in both subdomains. The capillary pressure-saturation functions are

$$\pi^{(l)} = 5(1 - s_w)^2, \quad \pi^{(r)} = 4(1 - s_w)^2 + 1 \quad (30)$$

resulting in a critical saturation $s_w^* = 1/\sqrt{5}$. These functions are somewhat unusual and the fact $\frac{d}{ds_w}\pi^{(i)}(1) = 0$ results in an infinite slope of the inverse capillary pressure-saturation relationship ψ at entry pressure. Therefore, $\psi^{(i)}$ is regularized for $p_c < \tilde{p}_e^{(i)} = \pi^{(i)}(1) + 10^{-2}$ by a straight line in a C^1 fashion.

The boundary conditions are $\phi_{wh}(0) = 1.8$, $\phi_{wh}(2) = 0$, $\phi_{ch}(0) = 0$, $\nu \cdot v_n(2) = 0$ and the initial conditions are

$$\phi_{ch}(x) = \begin{cases} 5 \cdot (0.9)^2 & 0.1 < x < 0.9 \\ 1 & x > 1 \\ 0 & \text{else} \end{cases}.$$

Figure 2 shows the non-wetting phase saturation at various times obtained with polynomial degree $p = 1$ and the second-order Alexander scheme. Time steps were equidistant and are given in the figure legend. Due to the pressure gradient the non-wetting phase is pushed to the right. When the critical saturation is reached the right subdomain is infiltrated and a saturation discontinuity persists at the media interface. The left front moves to the left since capillary diffusion dominates the convective flux, at least initially. As in the first test case we observe convergence of the solution under mesh refinement and a corresponding reduction of the oscillations in the vicinity of the free boundary.

In comparison with the results given in [40, 41] we see less variations between the solutions on different refinement levels indicating that the solution is more accurate already on coarser grids. Computations with first-order fully-implicit Euler (not provided) did not show significant differences which suggests that this error might be a splitting error of the

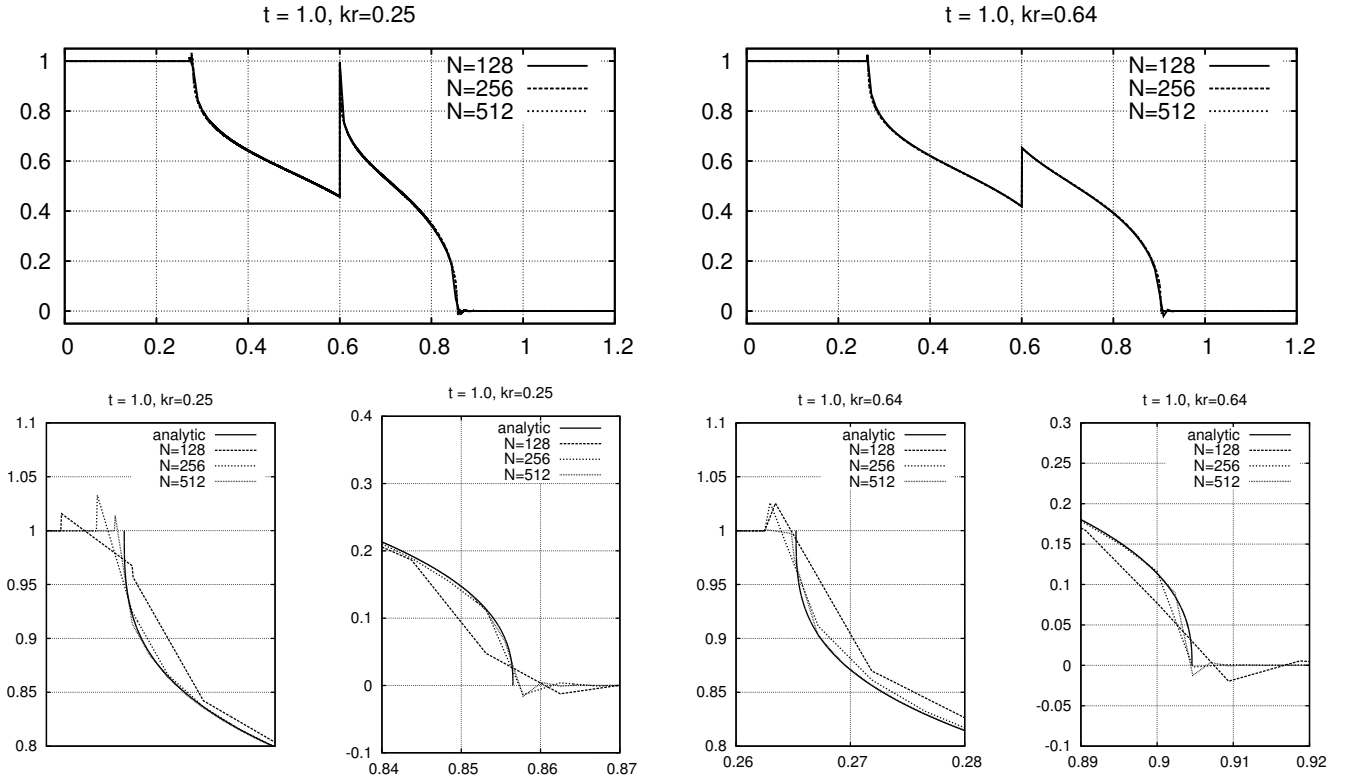


Figure 1: Wetting phase saturation in test case 1 at time $t = 1$. First row shows case 1a (left) and case 1b (right). Second row shows details of the solution close to the free boundary for case 1a and 1b.

decoupled scheme. Moreover, we emphasize again that the results in Figure 2 were obtained without $H(\text{div})$ reconstruction.

5.4 Test Case 3: 2d DNAPL Infiltration

In this section we consider a two-dimensional (vertical) DNAPL infiltration problem with two different rock types similar to the one described in [11]. This problem tests the ability of the method to realize the interface conditions, handling of gravitational effects and various boundary conditions. The quality of the solution on coarse meshes, its scalability to very fine meshes and the performance relative to a cell-centered finite volume scheme are also evaluated.

5.4.1 Problem Setup

The geometry and boundary conditions are given in Figure 4. At the inflow boundary on the top a flux of $0.075 [kg s^{-1} m^{-2}]$ of the non-wetting phase into the domain is prescribed. At all other parts of the top and bottom boundary no flow conditions are prescribed for both phases (at the inflow boundary no flow is also prescribed for the wetting phase). At the left and right boundary full saturation of the wetting phase, $s_w = 1$, and hydrostatic conditions for the pressure p_w are prescribed.

Table 2: Parameters for the two rock types in the DNAPL infiltration problem.

Parameter	Rock type 1	Rock type 2
Porosity Φ	0.4	0.4
Abs. perm. $K [m^2]$	$6.64 \cdot 10^{-11}$	$3.32 \cdot 10^{-11}$
rel. perm.	quadratic, see text	
$p_e [Pa]$	755	1163
λ	2.5	2

The mass densities of the fluids are $\rho_w = 1000 [kg m^{-3}]$ and $\rho_n = 1460 [kg m^{-3}]$ while the dynamic viscosities are $\mu_w = 10^{-3} [Pa s]$ and $\mu_n = 0.9 \cdot 10^{-3} [Pa s]$. The relative permeabilities are chosen as quadratic functions and are the same for both rock types:

$$k_{rw}(s_w) = s_w^2, \quad k_{rn}(s_n) = s_n^2.$$

If $s_\alpha < 0$ we set $k_{r\alpha}(s_\alpha) = 0$ and if $s_\alpha > 1$ we set $k_{r\alpha}(s_\alpha) = 1$. The capillary pressure saturation function is of Brooks-Corey type with parameters given in Table 2 and the regularization given in (29) is applied with $R = 4$. Finally, porosity and absolute permeability are given in Table 2 as well.

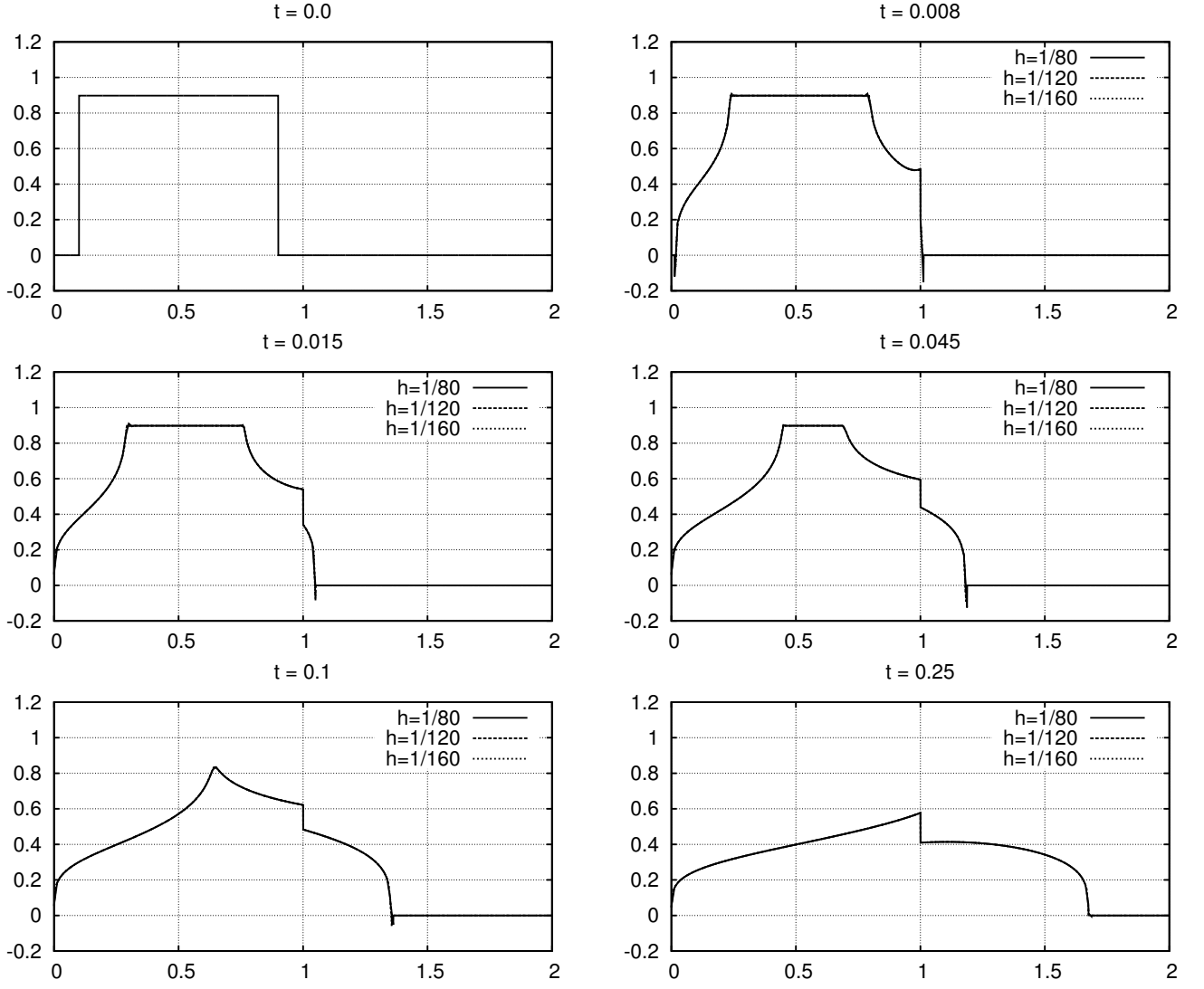


Figure 2: Comparison of saturation of non-wetting phase in test case 2 for different mesh sizes. Time step size was $\Delta t = 1 \cdot 10^{-3}$ for $h = 1/80$, $\Delta t = 5 \cdot 10^{-4}$ for $h = 1/120$ and $\Delta t = 2.5 \cdot 10^{-4}$ for $h = 1/160$. Solution is shown at times $t = 0, 0.008, 0.015, 0.045, 0.1, 0.25$ (from top to bottom, left to right).

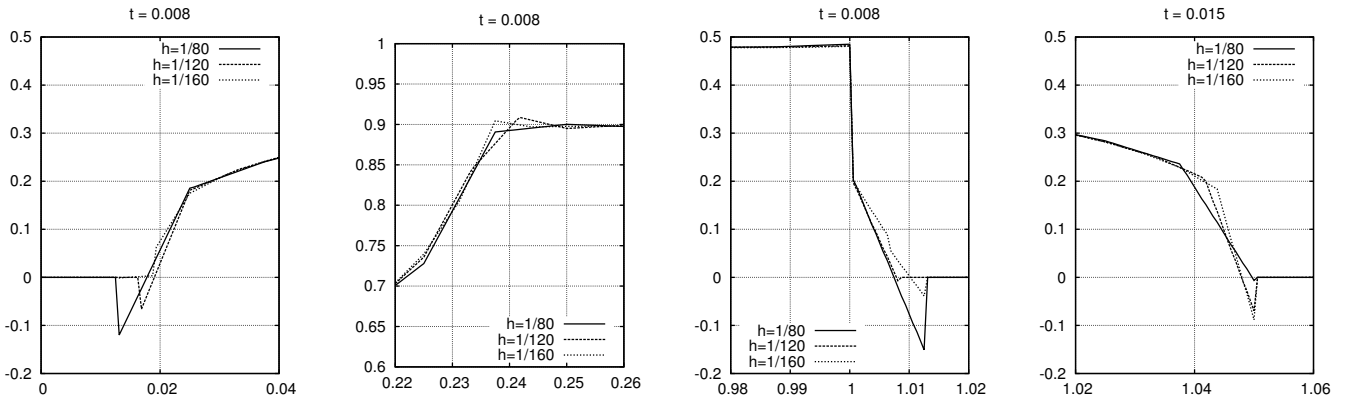


Figure 3: Details of the solutions in test case 2. From left to right: Bottom part of left front at $t = 0.008$, upper part of left front at $t = 0.008$, bottom part of right front at $t = 0.008$, bottom part of right front at $t = 0.015$.

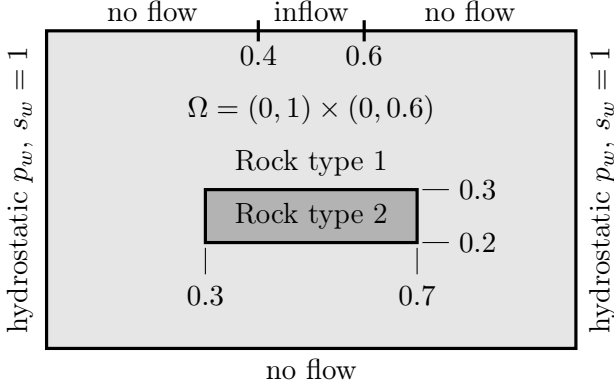


Figure 4: Geometry and boundary conditions for the DNAPL infiltration problem.

5.4.2 Accuracy on Coarse Meshes

Discontinuous Galerkin schemes (of high order) are more expensive in terms of degrees of freedom and computation time compared to simple low order schemes. Therefore it is of particular interest to see the performance on relatively coarse meshes. In Figure 5 we compare the non-wetting phase saturation obtained with DG/ \mathbb{P}_1 , DG/ \mathbb{P}_2 , DG/ \mathbb{Q}_1 and DG/ \mathbb{Q}_2 with a cell-centered finite volume scheme (CCFV) using either full-upwinding or central evaluation of mobilities. The CCFV scheme is based on a wetting-phase pressure / capillary pressure formulation with harmonic permeability weighting (where relative permeabilities are either evaluated with the upwind saturation or the arithmetically averaged saturation, cf. [60] for details).

In Figure 5 consider the first row of images. From the left we have DG/ \mathbb{P}_1 on an unstructured mesh consisting of 120 triangles generated with Gmsh [47] in the middle DG/ \mathbb{Q}_1 on a structured, equidistant mesh consisting of 60 quadrilaterals and on the right the CCFV upwind scheme on the structured mesh being uniformly refined to 240 elements. The meshes have been chosen such that they correspond roughly to the same number of spatial degrees of freedom (in the case of DG/ \mathbb{Q}_1 and CCFV they are identical). In the second and third row the same schemes are shown on uniformly refined meshes. In rows 4–6 we show results for DG/ \mathbb{P}_2 (left column), DG/ \mathbb{Q}_2 (middle column) and CCFV with central evaluation of capillary pressure (right column). All results are shown for $T = 3600s$ while a different number of timesteps have been performed keeping $\Delta t/h$ fixed. In addition, implicit Euler has been employed for upwind CCFV while the second order Alexander scheme [2] was used for all other spatial discretizations. In Table 3 the minimum and maximum of the numeri-

cal solution for the different schemes and meshes are given.

From these results we can conclude:

- On the coarsest meshes the lowest order DG schemes exhibit severe undershoots. These negative saturations are always located in the vicinity of the free boundary and they are reduced as the mesh is refined. The CCFV upwind scheme is monotone as expected and the CCFV central scheme shows small undershoots that are quickly reduced as the mesh is refined.
- On the coarsest meshes (first row) the DG schemes are quite accurate above, within and below the low permeability lense in comparison to the CCFV upwind scheme. This is also supported by the maximum of the numerical solutions (which is attained in the midpoint of the upper boundary of the lense). Both CCFV schemes are less accurate (given the same number of degrees of freedom) with respect to the maximum value.
- Increasing the polynomial degree in the DG scheme gives a considerable improvement of the solution, also with respect to the undershoots and the maximum.

5.4.3 Accuracy on Fine Meshes

The DNAPL infiltration problem is now solved on meshes with up to 2560×1536 elements for the CCFV scheme. Since no analytical solution is available we plot 1D profiles along the vertical line $x = 0.5$ at the final time $T = 3600$ for various schemes, mesh resolutions and time step sizes. The time step size is always chosen such that $\Delta t/h = \text{const.}$ The number of time steps is listed in Table 5.

Figure 6 (top left) shows the overall profile with the DNAPL pooling up in the interval $z \in (0.3, 0.6)$, the upper interface at $z = 0.3$ where DNAPL infiltrates the low permeability lense, the region $z \in (0.2, 0.3)$ within the low permeability lense, the lower interface $z = 0.2$ where DNAPL exfiltrates the lense and finally the free boundary near position $z \approx 0.09$. At the lower interface the saturation s_n is zero from inside the lense and capillary pressure is discontinuous since the critical saturation is not attained outside the lense. Clearly, at the resolution shown, the solutions obtained with DG/ \mathbb{Q}_1 and DG/ \mathbb{Q}_2 as well as the second-order CCFV scheme coincide well. In order to compare the schemes in detail we look at the solution close to the free boundary.

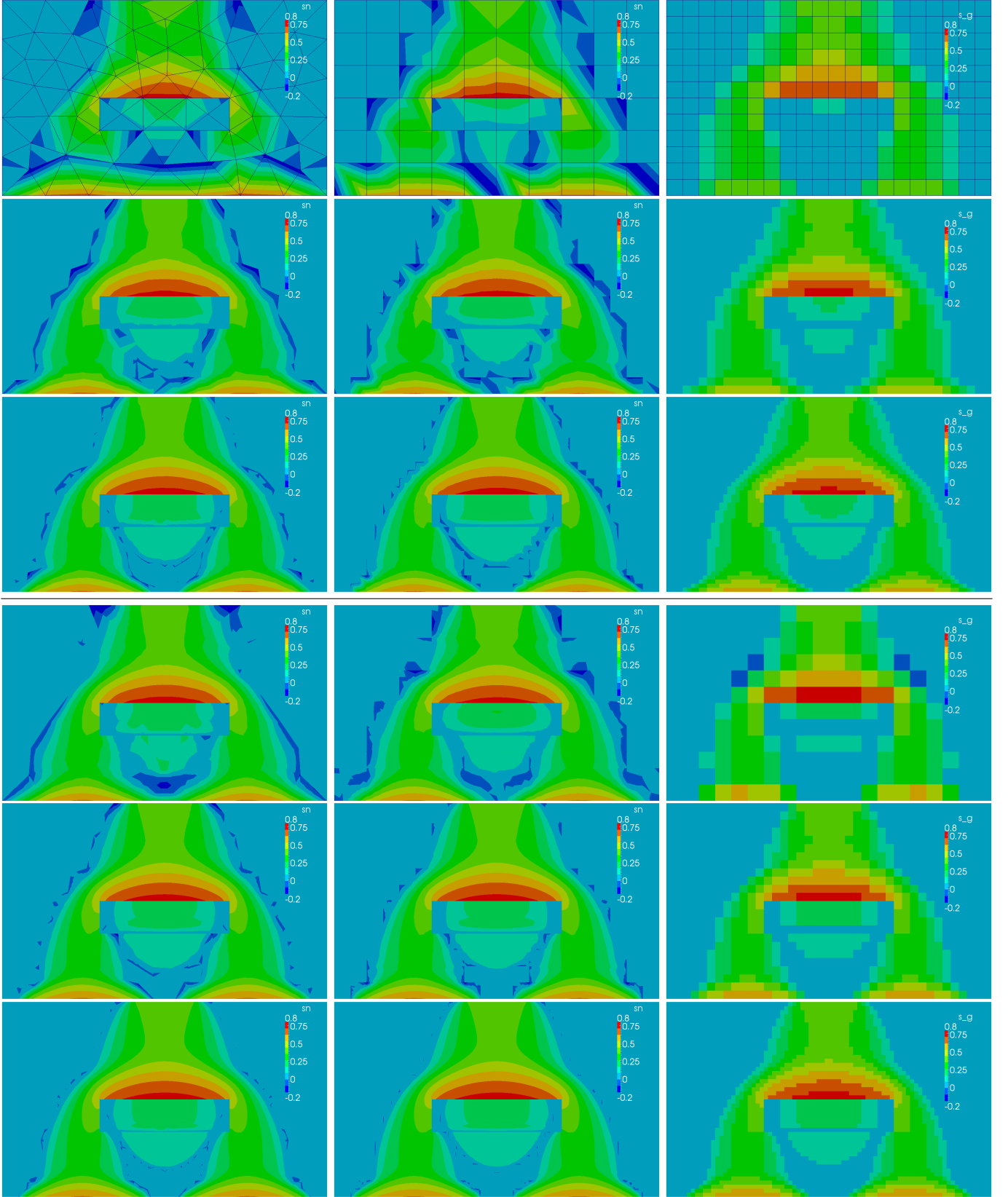


Figure 5: Comparison of non-wetting phase saturation for different schemes on coarse grids. First set of three rows: Left column shows DG/P_1 on unstructured triangular meshes with 120, 498 and 1474 elements, middle column shows DG/Q_1 on structured, equidistant meshes with 60, 240 and 960 elements, right column shows upwind CCFV scheme on structured, equidistant meshes with 240, 960 and 3840 elements. Second set of three rows: DG/P_2 (left column), DG/Q_2 (middle column), second order CCFV (right column) on the same meshes as first set.

Table 3: Minima and maxima of the non-wetting phase saturation corresponding to the images shown in Figure 5. Note that for each scheme results for one additional level of refinement is given.

DG/ \mathbb{P}_1			DG/ \mathbb{Q}_1			CCFV upwind		
Elements	min	max	Elements	min	max	Elements	min	max
120	-0.57	0.7416	60	-0.51	0.7555	240	0	0.7022
498	-0.32	0.7461	240	-0.20	0.7489	960	0	0.7248
1474	-0.20	0.7493	960	-0.17	0.7501	3840	0	0.7367
7182	-0.14	0.7503	3840	-0.10	0.7505	15360	0	0.7434

DG/ \mathbb{P}_2			DG/ \mathbb{Q}_2			CCFV central		
Elements	min	max	Elements	min	max	Elements	min	max
120	-0.39	0.7488	60	-0.19	0.7555	240	-0.14	0.7243
498	-0.23	0.7499	240	-0.20	0.7489	960	$-2.0 \cdot 10^{-2}$	0.7347
1474	-0.14	0.7505	960	-0.10	0.7501	3840	$-1.0 \cdot 10^{-2}$	0.7417
7182	-0.10	0.7507	3840	$-8.5 \cdot 10^{-2}$	0.7505	15360	$-5.6 \cdot 10^{-3}$	0.7459

The right plot in the upper row of Figure 6 provides a comparison of the first and second order CCFV schemes. The implicit Euler / full upwind scheme is very diffusive and even the coarsest solution obtained with the second-order scheme that is shown (320×192) exhibits a better position of the free boundary than the first-order scheme on a three times refined grid. Therefore we do not consider the first-order method any further in the sequel.

The plots in the bottom row of Figure 6 compare the second-order DG/ \mathbb{Q}_1 scheme with the second-order CCFV scheme. The results show that DG/ \mathbb{Q}_1 on a given mesh is as accurate as the solution obtained with second-order CCFV on a two-times refined mesh. Since CCFV on a two times refined mesh has four times (eight in 3D) the number of degrees of freedom and needs two times more time steps (see Table 5) the DG scheme is more efficient in terms of number of degrees of freedom.

5.4.4 Comparison of Solver Performance and Overall Computation Time

First we would like to illustrate the need for efficient linear solvers. For that reason Table 4 compares the performance of two different linear solvers, the BiCGStab method preconditioned by block ILU (blocks corresponding to all degrees of freedom associated with a mesh element) and the hybrid AMG/DG preconditioner presented in Section 4. 10 time steps of the DNAPL infiltration problem have been computed with the DG/ \mathbb{Q}_1 scheme and $\Delta t/h$ fixed. The table lists the number of spatial degrees of freedom, the average number of preconditioner evalua-

tions per Newton step (ALIN), the maximum number of preconditioner evaluations in one Newton step (MAXLIN) and the total computation time (TT) in seconds (including Jacobian assembly) on one Intel Core i7 processor running at 2.6 GHz. The single grid preconditioner clearly shows the expected doubling of the number of iterations while the AMG preconditioner needs a constant average number of iterations and the maximum number slowly increasing. With respect to total computation time, the single grid method is faster or comparable to the AMG preconditioner up to 30000 degrees of freedom. At 500000 degrees of freedom the AMG method is faster by a factor of two in total computation time. Note that on the finest mesh about 700s are used for Jacobian assembly meaning that the AMG solver alone is about 3.5 times faster.

Table 5 now provides more details of the simulation runs for test case 3 reported in Subsection 5.4.3 including total computation times. All computations have been performed with the cluster system Helics3a at Heidelberg university which consists of 32 nodes with four AMD Opteron 6212 (Interlagos) processors operating at 2.6 GHz and connected by a Mellanox 40G QDR infiniband network. Each processor has eight cores resulting in 1024 cores for the full machine.

In the previous Subsection we concluded that the DG solution on the 320×192 mesh is as accurate as the CCFV solution on the 1280×768 mesh. The total computation time for the DG scheme on 64 cores was 3251s compared to 6496s for the CCFV scheme on the same number of cores. DG on the 640×392 mesh compares to CCFV on the 2560×1536 mesh with

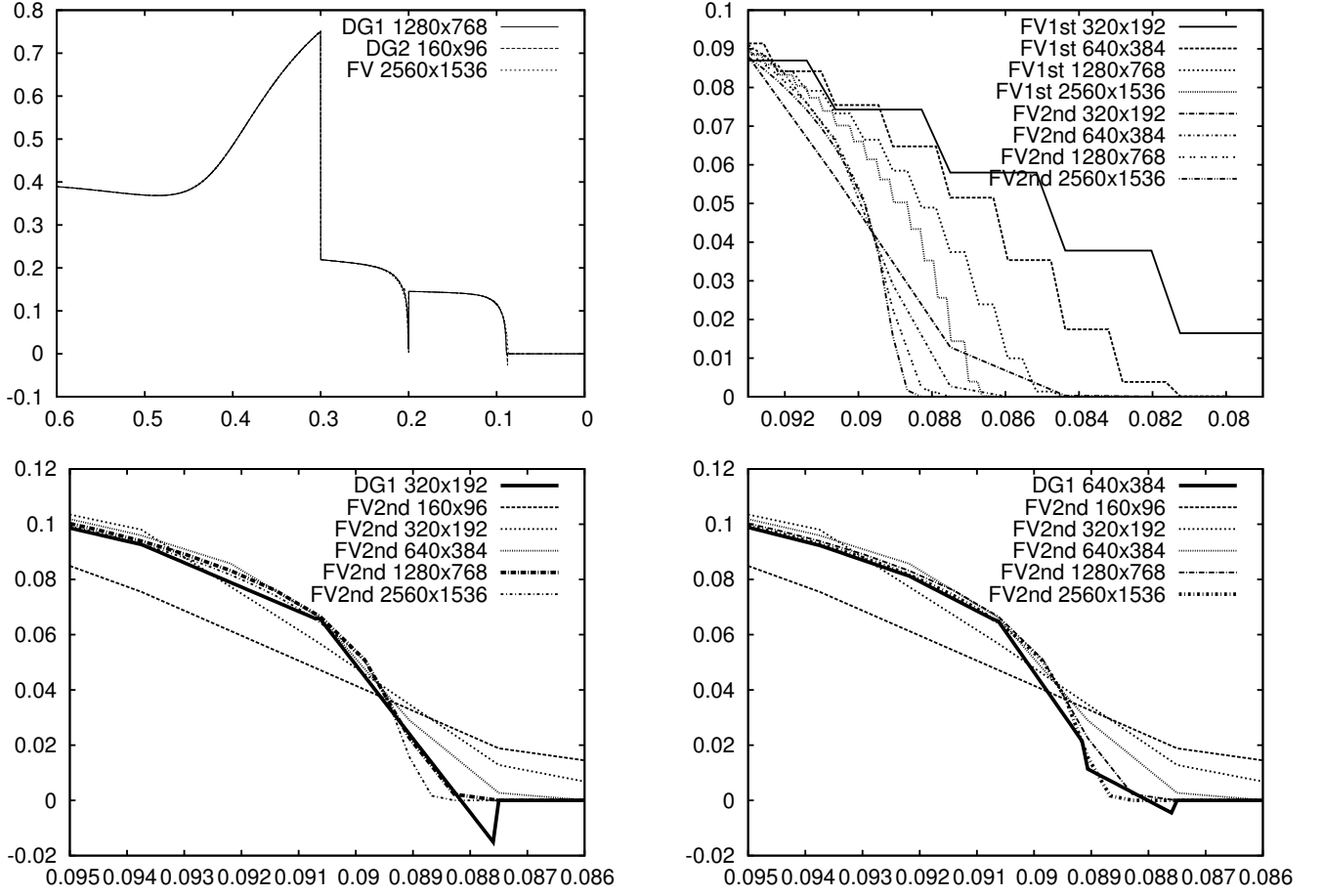


Figure 6: Comparison of non-wetting phase saturation over z position at $x = 0.5$ in test case 3. Top left: Complete profile along the line $x = 0.5$ for DG and CCFV scheme on fine meshes. Top right: Zoom of region near the free boundary and comparison of first and second order CCFV schemes. Bottom left: Comparison of DG scheme on 320×192 mesh with second order CCFV. Bottom right: Comparison of DG scheme on 640×384 mesh with second order CCFV.

Table 4: Comparison of two iterative solvers for the DNAPL infiltration problem.

DOF	BiCGStab-ILU			BiCGStab-Hybrid AMG		
	ALIN	MAXLIN	TT	ALIN	MAXLIN	TT
480	33.0	58	0.7	2.8	4	0.9
1920	54.2	107	3	2.2	4	3.8
7680	91.0	223	14	2.0	2	19.0
30720	152.2	459	71	2.3	4	66.7
122880	231.0	773	408	2.6	8	272.8
491520	353.4	1945	2083	2.8	8	1114.9

corresponding total computation times of 11233s and 12775s on 256 cores. This shows that the DG scheme can provide an advantage compared to the CCFV scheme even in the most relevant measure which is total computation time.

The less favourable comparison of both schemes on the finer grid is due to the worse scalability of the AMG/DG preconditioner compared the AMG preconditioner applied to the linear systems arising in the CCFV scheme. The column labeled ALIN reports the average number of preconditioner steps per Newton step. Clearly, the AMG preconditioner is more robust for the CCFV scheme. The time needed for one application of the preconditioner is shown in the column labeled LTIT. It shows that the time per iteration scales slightly better for the DG scheme than for CCFV which might be due to better data locality of the DG scheme.

Finally, Table 5 illustrates that the fully-coupled DG scheme with half the time step size needs roughly the same number of Newton iterations as the fully-coupled CCFV scheme on the same mesh. This confirms that the nonlinear systems arising from the DG discretization can be solved as efficiently as in the finite volume case.

5.5 Test Case 4: DNAPL Infiltration in Random Porous Medium

In order to illustrate that the DG scheme is able to handle more difficult problems and also performs well in three space dimensions we applied it to DNAPL infiltration into a random porous medium with log-normally distributed absolute permeability with correlation length $6h$ in x -direction and $3h$ in z -direction (h is the mesh size). The variance has been chosen such that permeability varied about by about 1.5 orders of magnitude in the two-dimensional example and one order of magnitude in the three-dimensional example. The capillary pressure-saturation function is of Brooks-Corey type with $\lambda = 2.5$ and entry pressure is scaled with permeability

$$\pi(s_w, x) = \sqrt{\bar{K}/K(x)} s_w^{-1/\lambda}$$

where \bar{K} is the mean of the permeability field. This results in a different entry pressure for each mesh element.

Figures 7 and 8 show the results obtained with the DG/ Q_1 scheme at various times. Clearly, capillary heterogeneity has a strong influence on the saturation distribution even for relatively mild variations in absolute permeability. Additional information on these simulations is shown in Table 6. The 2D simulation

used two million spatial degrees of freedom and computed about 12000 time steps on 512 processors in about 8h total computation time. The 3D simulation used nearly 100 million spatial degrees of freedom and performed about 1000 time steps which took about 100h total computation time on 1024 processors. It is interesting to note that in the 3D simulation the ratio of time spent for assembling the Jacobians to time spent for solving the linear systems (last column in Table 6) was 1.4 while for the 2D simulation it was 0.5.

6 CONCLUSION

In this work a new fully-coupled discontinuous Galerkin scheme for the two-phase flow problem based on a formulation with wetting-phase potential and capillary potential as primary variables is presented. By way of numerical experiment it is shown that (i) the scheme is as accurate as a cell-centered finite volume scheme on a two times refined grid, (ii) no $H(\text{div})$ reconstruction of the velocity is necessary in the fully-coupled scheme in contrast to some decoupled schemes and (iii) an efficient parallel algebraic multigrid preconditioner for the fully-coupled two-phase DG system is available. Even when compared to the very cheap cell-centered scheme significant speedups w.r.t. total computation time can be achieved. In this comparison it should be taken into account that DG is a much more flexible approach that is able to handle unstructured, non-conforming grids, hp -adaptivity and full tensor permeabilities. Problems with up to about 100 million degrees of freedom in three space dimension are solved on 1000 cores. Future work should include a numerical comparison with pressure-saturation based formulations as well as decoupled formulations.

Acknowledgements This work would not have been possible without the wonderful effort of the DUNE developer community during the last decade. There devotion to producing high quality open-source software is greatly appreciated. I also thank Olaf Ippisch for many fruitful discussions about pressure-pressure based methods for two-phase flow.

REFERENCES

- [1] V. Aizinger, C. Dawson, B. Cockburn, and P. Castillo. The local discontinuous Galerkin method for contaminant transport. *Adv. Wat. Res.*, 24:73–87, 2001.
- [2] R. Alexander. Diagonally implicit Runge-Kutta

Table 5: Weak scalability results for test case 3. P is the number of processors used, h^{-1} is the mesh size, DOF is the number spatial degrees of freedom, TS is the number of successful time steps need to reach the final time $T = 3600s$, ANL is the average number of Newton iterations per (successful) time step, ALIN is the average number of preconditioner steps needed per linear solve, TT is the total computation time in seconds and LTIT is the time for one application of the preconditioner.

Scheme	P	h^{-1}	DOF	TS	ANL	ALIN	TT	LTIT
DG/ \mathbb{Q}_1	1	40	$7.7 \cdot 10^3$	30	11.4	1.8	156.8	0.144
	4	80	$3.1 \cdot 10^4$	71	11.0	3.4	466.1	0.052
	16	160	$1.2 \cdot 10^5$	125	12.0	5.7	1187.3	0.062
	64	320	$4.9 \cdot 10^5$	263	11.4	9.1	3250.5	0.067
	256	640	$2.0 \cdot 10^6$	563	10.7	15.3	11233.0	0.082
	1024	1280	$7.9 \cdot 10^6$	1369	9.2	17.0	41917.4	0.112
2nd order	1	160	$3.1 \cdot 10^4$	60	7.7	1.8	191.2	0.043
CCFV	4	320	$1.2 \cdot 10^5$	120	8.2	2.2	592.1	0.069
	16	640	$4.9 \cdot 10^5$	246	8.4	2.6	1453.7	0.078
	64	1280	$2.0 \cdot 10^6$	491	8.9	3.3	6496.1	0.151
	256	2560	$7.9 \cdot 10^6$	1021	9.7	4.5	12774.9	0.156

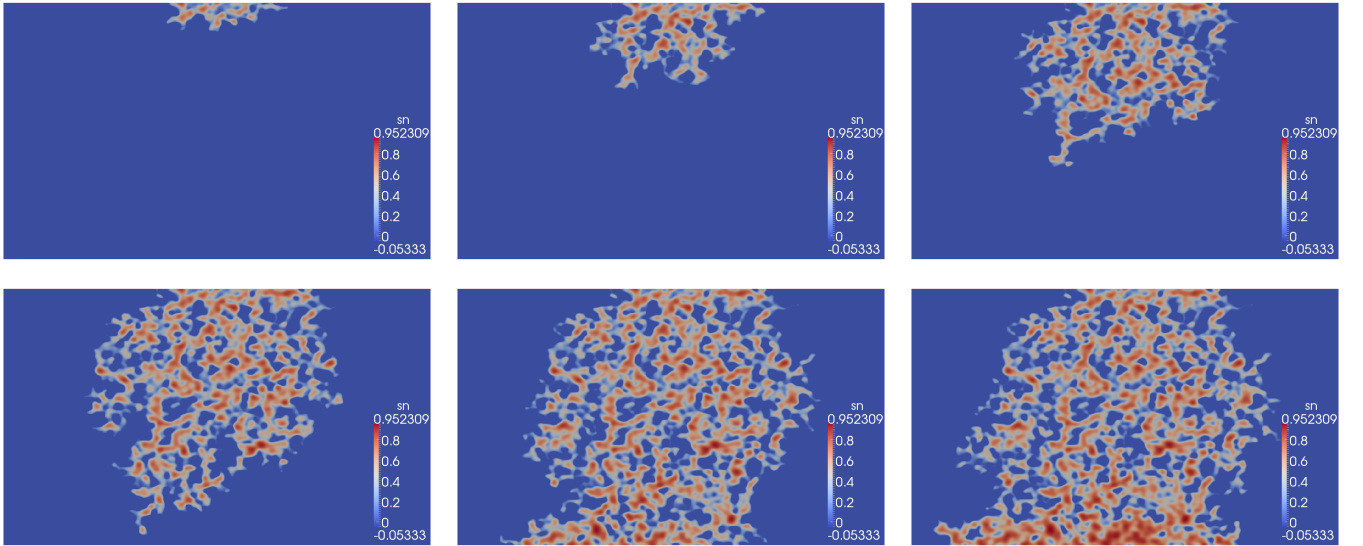


Figure 7: 2D DNAPL infiltration into a porous medium with random permeability and entry pressure. Images show saturation of non-wetting phase.

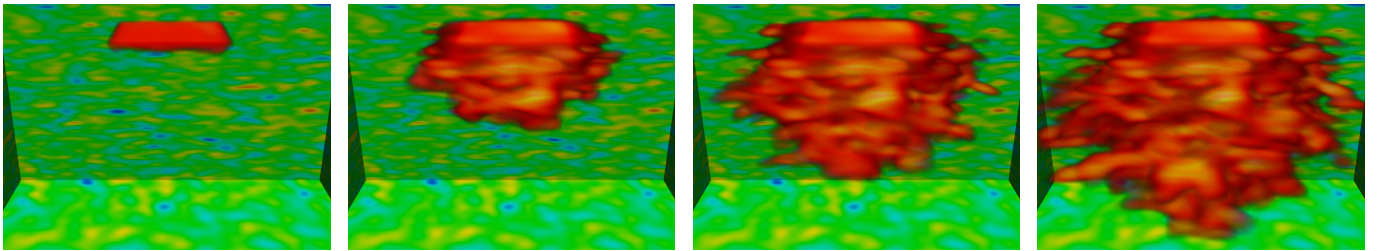


Figure 8: 3D DNAPL infiltration into a porous medium with random permeability and entry pressure. Images show volume rendering of non-wetting phase saturation in red and the absolute permeability on the sides of the cube.

Table 6: Simulation data for the random DNAPL infiltration problem (test case 4).

Problem	P	DOF	TS	ANL	ALIN	TT [h]	ASS/SLV
2D	512	$2 \cdot 10^6$	12019	4.1	2.5	8.3	0.5
3D	1024	$8.8 \cdot 10^7$	1026	6.0	4.3	107.0	1.4

- methods for stiff O. D. E.'s. *SIAM Journal on Numerical Analysis*, 14(6):1006–1021, 1977.
- [3] D. N. Arnold, F. Brezzi, B. Cockburn, and L. D. Marini. Unified analysis of discontinuous Galerkin methods for elliptic problems. *SIAM J. Numer. Anal.*, 39(5):1749–1779, 2002.
- [4] B. Ayuso De Dios, M. Holst, Yunrong Zhu, and L.T. Zikatanov. Multilevel preconditioners for discontinuous Galerkin approximations of elliptic problems with jump coefficients. Technical report, arXiv:1012.1287, 2011.
- [5] K. Aziz and A. Settari. *Petroleum Reservoir Simulation*. Elsevier, 1979.
- [6] P. Bastian. Numerical computation of multiphase flow in porous media. Habilitationsschrift, 1999.
- [7] P. Bastian. Higher order discontinuous Galerkin methods for flow and transport in porous media. In E. Bänsch, editor, *Challenges in Scientific Computing – CISC 2002*, volume 35 of *Lecture Notes in Computational Science and Engineering*, pages 1–22. Springer, 2003.
- [8] P. Bastian, M. Blatt, A. Dedner, C. Engwer, R. Klöforn, R. Kornhuber, M. Ohlberger, and O. Sander. A generic grid interface for parallel and adaptive scientific computing. part II: implementation and tests in DUNE. *Computing*, 82(2-3):121–138, 2008.
- [9] P. Bastian, M. Blatt, A. Dedner, C. Engwer, R. Klöforn, M. Ohlberger, and O. Sander. A generic grid interface for parallel and adaptive scientific computing. part I: abstract framework. *Computing*, 82(2-3):103–119, 2008.
- [10] P. Bastian, F. Heimann, and S. Marnach. Generic implementation of finite element methods in the distributed and unified numerics environment (DUNE). *Kybernetika*, 46(2):294–315, 2010.
- [11] P. Bastian and R. Helmig. Efficient fully-coupled solution techniques for two-phase flow in porous media: Parallel multigrid solution and large scale computations. *Adv. Water Res.*, 23:199–216, 1999.
- [12] P. Bastian and S. Lang. Couplex benchmark computations with UG. *Computational Geosciences*, 8(2):125–147, 2004.
- [13] P. Bastian and B. Rivière. Superconvergence and H(div)-projection for discontinuous Galerkin methods. *Int. J. Numer. Meth. Fluids.*, 42(10):1043–1057, 2003.
- [14] P. Bastian and B. Rivière. Discontinuous galerkin methods for two-phase flow in porous media. Technical Report 2004-28, IWR, University of Heidelberg, 2004.
- [15] Peter Bastian, Markus Blatt, and Robert Scheichl. Algebraic multigrid for discontinuous galerkin discretizations of heterogeneous elliptic problems. *Numerical Linear Algebra with Applications*, 19(2):367–388, 2012.
- [16] J. Bear. *Dynamics of Fluids in Porous Media*. Dover Publications, 1972.
- [17] M. Bertsch, R. Passo, and C. Van Duijn. Analysis of oil trapping in porous media flow. *SIAM Journal on Mathematical Analysis*, 35(1):245–267, 2003.
- [18] Markus Blatt. *A Parallel Algebraic Multigrid Method for Elliptic Problems with Highly Discontinuous Coefficients*. PhD thesis, Ruprecht-Karls-Universität Heidelberg, 2010.
- [19] Alain Bourgeat, Mladen Jurak, and Farid Smaï. Two-phase, partially miscible flow and transport modeling in porous media; application to gas migration in a nuclear waste repository. *Computational Geosciences*, 13(1):29–42, 2009.
- [20] D. Braess. Towards algebraic multigrid for elliptic problems of second order. *Computing*, 55:379–393, 1995.
- [21] Konstantin Brenner, Clément Cancès, and Danielle Hilhorst. Finite volume approximation for an immiscible two-phase flow in porous media with discontinuous capillary pressure. *Computational Geosciences*, 17(3):573–597, 2013.
- [22] Susanne C. Brenner and Jie Zhao. Convergence of multigrid algorithms for interior penalty methods. *Applied Numerical Analysis and Computational Mathematics*, 2(1):3–18, 2005.
- [23] R. H. Brooks and A. T. Corey. *Hydraulic Properties of Porous Media*, volume 3 of *Colorado State University Hydrology Paper*. Colorado State University, 1964.
- [24] Fulvia Buzzi, Michael Lenzinger, and Ben Schweizer. Interface conditions for degenerate two-phase flow equations in one space dimension. *Analysis*, 29(3):299–316, 2009.
- [25] C. Cancès, T. Gallouët, and A. Porretta. Two-phase flows involving capillary barriers in heterogeneous porous media. *Interfaces and Free Boundaries*, 11:239–258, 2009.

- [26] C. Cancès and M. Pierre. An existence result for multidimensional immiscible two-phase flows with discontinuous capillary pressure field. *SIAM Journal on Mathematical Analysis*, 44(2):966–992, 2012.
- [27] Clément Cancès. Finite volume scheme for two-phase flows in heterogeneous porous media involving capillary pressure discontinuities. *ESAIM: Mathematical Modelling and Numerical Analysis*, 43:973–1001, 9 2009.
- [28] G. Chavent and J. Jaffré. *Mathematical Models and Finite Elements for Reservoir Simulation*. North-Holland, 1978.
- [29] Holger Class, Anozie Ebigbo, Rainer Helmig, Helge K. Dahle, Jan M. Nordbotten, Michael A. Celia, Pascal Audigane, Melanie Darcis, Jonathan Ennis-King, Yaqing Fan, Bernd Flemisch, Sarah E. Gasda, Min Jin, Stefanie Krug, Diane Labregere, Ali Naderi Beni, Rajesh J. Pawar, Adil Sbai, Sunil G. Thomas, Laurent Trenty, and Lingli Wei. A benchmark study on problems related to CO₂ storage in geologic formations. *Computational Geosciences*, 13(4):409–434, 2009.
- [30] B. Cockburn, S. Y. Lin, and C.-W. Shu, editors. *Discontinuous Galerkin methods. Theory, computation and applications*, volume 11 of *Lecture Notes in Computational Science and Engineering*. Springer-Verlag, 2000.
- [31] B. Cockburn and C.-W. Shu. The local discontinuous Galerkin finite element method for convection-diffusion systems. *SIAM J. Numer. Anal.*, 35:2440–2463, 1998.
- [32] B. Cockburn and C.-W. Shu. The Runge-Kutta discontinuous Galerkin method for conservation laws V: Multidimensional systems. *J. Comput. Phys.*, 141:199–224, 1998.
- [33] M. J. de Neef and J. Molenaar. Analysis of DNAPL infiltration in a medium with a low permeable lense. *Computational Geosciences*, 1:191–214, 1997.
- [34] Daniele Antonio Di Pietro and Alexandre Ern. *Mathematical Aspects of Discontinuous Galerkin Methods*. Springer, 2012.
- [35] Daniele Antonio Di Pietro, Alexandre Ern, and Jean-Luc Guermond. Discontinuous galerkin methods for anisotropic semidefinite diffusion with advection. *SIAM J. Numer. Anal.*, 2008.
- [36] C.J. Duijn, J. Molenaar, and M.J. de Neef. The effect of capillary forces on immiscible two-phase flow in heterogeneous porous media. *Transport Porous Media*, 21:71–93, 1995.
- [37] C.J. Duijn, J. Molenaar, and M.J. de Neef. Similarity solution for capillary redistribution of two phases in a porous medium with a single discontinuity. *Adv. Water Res.*, 21:451–461, 1998.
- [38] Y. Epshteyn and B. Rivière. Fully implicit discontinuous finite element methods for two-phase flow. *Applied Numerical Mathematics*, 57(4):383 – 401, 2007.
- [39] A. Ern, I. Mozolevski, and L. Schuh. Accurate velocity reconstruction for discontinuous galerkin approximations of two-phase porous media flows. *C.R. Acad. Sci. Paris, Ser. I*(9–10):551–554, 2009.
- [40] A. Ern, I. Mozolevski, and L. Schuh. Discontinuous galerkin approximation of two-phase flows in heterogeneous porous media with discontinuous capillary pressures. *Computer Methods in Applied Mechanics and Engineering*, 199(23–24):1491 – 1501, 2010.
- [41] A. Ern, I. Mozolevski, and L. Schuh. Corrigendum to “Discontinuous Galerkin approximation of two-phase flows in heterogeneous porous media with discontinuous capillary pressures” [comput. methods appl. mech. engrg. 199 (2010) 1491-1501]. *Computer Methods in Applied Mechanics and Engineering*, 245-246(0):348 – 349, 2012.
- [42] A. Ern, S. Nicaise, and M. Vohralík. An accurate $H(\text{div})$ flux reconstruction for discontinuous galerkin approximations of elliptic problems. *C. R. Math. Acad. Sci. Paris*, 2007.
- [43] Alexandre Ern and Igor Mozolevski. Discontinuous Galerkin method for two-component liquid-gas porous media flows. *Computational Geosciences*, 16(3):677–690, 2012.
- [44] Alexandre Ern, Annette F. Stephansen, and Paolo Zunino. A discontinuous Galerkin method with weighted averages for advection-diffusion equations with locally small and anisotropic diffusivity. *IMA Journal of Numerical Analysis*, 29(2):235–256, 2009.
- [45] O.J. Eslinger. *Discontinuous Galerkin finite element methods applied to two-phase, air-water flow problems*. PhD thesis, University of Texas at Austin,, 2005.
- [46] J. Fořt, J. Fürst, J. Halama, R. Herbin, and F. Hubert, editors. *Finite volumes for complex applications VI: Problems & perspectives*, volume 4 of *Proceedings in mathematics*. Springer, 2011.
- [47] Christophe Geuzaine and Jean-François Remacle. Gmsh: A 3-d finite element mesh generator with built-in pre- and post-processing facilities. *International Journal for Numerical Methods in Engineering*, 79(11):1309–1331, 2009.
- [48] J. Gopalakrishnan and G. Kanschat. A multilevel discontinuous Galerkin method. *Numerische Mathematik*, 95:527–550, 2003.
- [49] W. Hackbusch. *Multi-Grid Methods and Applications*. Springer-Verlag, 1985.
- [50] R. Helmig. *Multiphase Flow and Transport Processes in the Subsurface – A Contribution to the Modeling of Hydrosystems*. Springer-Verlag, 1997.
- [51] Rainer Helmig and Ralf Huber. Comparison of galerkin-type discretization techniques for two-phase flow in heterogeneous porous media. *Advances in Water Resources*, 21(8):697 – 711, 1998.

- [52] Hussein Hoteit and Abbas Firoozabadi. Numerical modeling of two-phase flow in heterogeneous permeable media with different capillarity pressures. *Advances in Water Resources*, 31(1):56 – 73, 2008.
- [53] P. Houston and R. Hartmann. An optimal order interior penalty discontinuous Galerkin discretization of the compressible Navier-Stokes equations. *J. Comp. Phys.*, 227:9670–9685, 2008.
- [54] Klaus Johannsen. Multigrid methods for nonsymmetric interior penalty discontinuous Galerkin methods. ICES Report 05-23, University of Texas at Austin, 2005.
- [55] W. Klieber and B. Rivière. Adaptive simulations of two-phase flow by discontinuous galerkin methods. *Comput. Meth. Appl. Mech. Engrg.*, 2006.
- [56] B. H. Kueper and E. O. Frind. Two-phase flow in heterogeneous porous media 1. model development. *Water Resources Research*, 27(6):1049–1057, 1991.
- [57] B. H. Kueper and E. O. Frind. Two-phase flow in heterogeneous porous media 2. model application. *Water Resources Research*, 27(6):1059–1070, 1991.
- [58] E.H. Mueller and R. Scheichl. Massively parallel solvers for elliptic PDEs in numerical weather- and climate prediction. arXiv:1307.2036, 2013.
- [59] D. Nayagum, G. Schäfer, and R. Mosé. Modelling two-phase incompressible flow in porous media using mixed hybrid and discontinuous finite elements. *Computational Geosciences*, 2004.
- [60] Rebecca Neumann, Peter Bastian, and Olaf Ippisch. Modeling and simulation of two-phase two-component flow with disappearing nonwetting phase. *Computational Geosciences*, pages 1–11, 2012.
- [61] Luke N. Olson and Jacob B. Schroder. Smoothed aggregation multigrid solvers for high-order discontinuous galerkin methods for elliptic problems. *Journal of Computational Physics*, 230(18):6959 – 6976, 2011.
- [62] D. W. Peaceman. *Fundamentals of Numerical Reservoir Simulation*. Elsevier, 1977.
- [63] Florian Prill, Maria Lukáčová-Medvid’ová, and Ralf Hartmann. Smoothed aggregation multigrid for the discontinuous Galerkin method. *SIAM Journal on Scientific Computing*, 31:3503–3528, 2009.
- [64] M. Raw. Robustness of coupled algebraic multigrid for the Navier–Stokes equations. Technical Report 96–0297, AIAA, 1996.
- [65] V. Reichenberger, H. Jakobs, P. Bastian, and R. Helmig. A mixed-dimensional finite volume method for multiphase flow in fractured porous media. *Adv. Wat. Res.*, 29(7):1020–1036, 2006.
- [66] B. Rivière. Numerical study of a discontinuous galerkin method for incompressible two-phase flow. In *Proceedings of ECCOMAS 2004*, volume 2, 2004.
- [67] B. Rivière, M. F. Wheeler, and V. Girault. Improved energy estimates for interior penalty, constrained and discontinuous Galerkin methods for elliptic problems I. *Comput. Geosci.*, 3:337–360, 1999.
- [68] Béatrice Rivière. *Discontinuous Galerkin methods for solving elliptic and parabolic equations*. SIAM, 2008.
- [69] J.W. Ruge and K. Stüben. Algebraic multigrid. In S. F. McCormick, editor, *Multigrid Methods*, chapter 4, pages 73–130. SIAM Philadelphia, 1987.
- [70] U. Trottenberg, C. W. Oosterlee, and A. Schuüller. *Multigrid*. Academic Press, 2001.
- [71] P. Vaněk, J. Mandel, and M. Brezina. Algebraic multigrid based on smoothed aggregation for second and fourth order problems. *Computing*, 56:179–196, 1996.
- [72] Markus Wolff, Yufei Cao, Bernd Flemisch, Rainer Helmig, and Barbara Wohlmuth. Multipoint flux approximation L-method in 3d: numerical convergence and application to two-phase flow in porous media. In P. Bastian, J. Kraus, R. Scheichl, and M. Wheeler, editors, *Simulation of Flow in Porous Media*, volume 12 of *Radon Series on Computational and Applied Mathematics*, pages 39–80. de Gruyter, 2013.
- [73] Jinchao Xu. Iterative Methods by Space Decomposition and Subspace Correction. *SIAM Review*, 34(4):581–613, 1992.